Networks and Heterogeneous Media

https://www.aimspress.com/journal/nhm

NHM, 19(2): 597–610.
DOI: 10.3934/nhm.2024026
Received: 15 April 2024
Revised: 28 May 2024
Accepted: 06 June 2024
Published: 12 June 2024

Research article

A continuum model for the tensegrity Maxwell chain

Luca Placidi[1], Julia de Castro Motta[2], Rana Nazifi Charandabi[3] and Fernando Fraternali[2,*]

[1] International Telematic University Uninettuno, 00186 Rome, Italy

[2] Department of Civil Engineering, University of Salerno, 84084 Fisciano(SA), Italy

[3] Department of Information Engineering, Electrical Engineering and Applied Mathematics (DIEM), University of Salerno, 84084 Fisciano (SA), Italy

* **Correspondence:** Email: f.fraternali@unisa.it.

Abstract: A recent study has presented a Maxwell mass–spring model for a chain formed by two different types of tensegrity prisms alternating with lumped masses. Such a model shows tensegrity theta prisms arranged in parallel with minimal regular prisms acting as resonant substructures. It features a tunable frequency bandgap response, due to the possibility of adjusting the width of the bandgap regions by playing with internal resonance effects in addition to mass and spring contrasts. This paper expands such research by presenting a continuum modeling of the tensegrity Maxwell chain, which is useful to conduct analytic studies and to develop finite element models of the plane wave dynamics of the investigated system. In correspondence to the high wave-length limit, i.e., in the low wave number regime, it is shown that the dispersion relations of the discrete and continuum models provide similar results. Analytic solutions to the wave dynamics of physical systems are presented, which validate the predictions of the bandgap response offered by the dispersion relation of the continuum model.

Keywords: Maxwell chain; discrete to continuum; bandgap response; tensegrity structures

1. Introduction

Mechanical metamaterials are engineered systems designed to create exotic materials, often prepared in laboratories using two or more components or phases. These materials exhibit unconventional mechanical properties not found in conventional materials [1]. Some notable examples include bandgap metamaterials composed of phononic crystals [2, 3], which can be designed to exhibit adjustable frequency intervals where the transmission of mechanical waves is not permitted [4, 5]. Tensegrity bandgap metamaterials are formed by alternating lumped masses with tensegrity units of different types, allowing for the creation of mass–spring systems that exhibit

tunable frequency bandgaps. These bandgaps can be adjusted by internal and external prestress, as well as by contrasts in mass and spring properties between their elements (refer, e.g., to [6] and references tharein).

In the case of a forced mass–spring chain, when the length of such a system is finite and/or when the presence of a boundary breaks the periodicity condition, it is well known that the Bloch–Floquet wave form solutions of the dynamic problem do not longer satisfy the equations of motion. Two alternative strategies are available to overcome such an issue. The first one consists of solving the ordinary differential equations of motion of the discrete system with aid of the competent initial conditions, and accounting for any kinematic restrictions [6]. Such a strategy is generally accurate, but has a computational disadvantage if the number of unit cells is very large. The second strategy consists of deriving a continuum model of the mass-spring system equipped with competent Partial Differential Equations (PDEs) and Boundary Conditions (BCs). Such an approach can be accurate, in the presence of a correct mathematical formulation, only when the wave-length is larger than the size ε of the unit cell. However it offers the advantage that the associated computational effort is either negligible in presence of analytical solutions to the equations of motion or dependent on the adopted mesh size in the case of finite element approximations.

This work develops a continuum model of the tensegrity mass–spring system recently proposed in [6] (see Section 2 for a review of this model). The approach that is followed moves on from the introduction of kinematic descriptors at the continuum level for the chain domain (i.e., 'hosting' and 'resonant' displacement fields) and next introduces appropriate Piola's ansatzes to link such descriptors to those corresponding to the discrete model [7–10]. The adopted ansatz guarantees that the continuum descriptors correspond to the limits for $\varepsilon \to 0$ of the discrete counterparts. Using the continuum displacement fields and a variational principle for the action functional system, the work derives the PDEs of the Maxwell chain as well as the dispersion relation at the continuum level (Section 3). Analytic solutions of the wave dynamics of the continuum model are presented in Section 4, which illustrate its main features and permit the validation of the dispersion relation presented in the previous section. The paper ends with concluding remarks and directions for future work in Section 5.

2. A tensegrity Maxwell chain model

We hereafter recall the main features of the tensegrity Maxwell chain model diffusely presented in [6], which is graphically illustrated in Figure 1. It is composed of a number of N tensegrity $\theta = 1$ prisms ('P_H prisms') [14] arranged in parallel with $2N$ minimal regular tensegrity prisms ('P_R prisms' or T3 prisms) [16]. The P_H prisms are interposed between $N + 1$ hosting masses M_H, while two P_R prisms are interposed between two consecutive M_H masses, being separated by a resonant M_R mass. The M_H and M_R masses exhibit characteristic sizes (r_H and r_R) and rotational moments of inertia $J_H = n_H M_H r_H^2$ and $J_R = n_R M_R r_R^2$ with respect to the axis of the chain, respectively, where n_H and n_R are two scalar factors depending on the shape of such elements ($n_H = n_R = 1/2$ in the case of masses consisting of circular discs with radii r_H and r_R).

The model analyzed hereafter describes the response of the chain in the small displacement regime from the reference configuration, by reducing the prism units to linear springs endowed with stiffness coefficients K_H (P_H prisms) and K_R (P_H prisms). The latter coincides with the tangent values of the

axial stiffness coefficients of the P_H and P_R prisms in correspondence to the reference configuration and are assumed to be positive. Let u_i^H denote the axial displacement of the $i-$th hosting mass and let ϑ_i^H denote the twisting rotation that accompanies the axial deformation of the P_H prism interposed between the hosting masses i and $i+1$. Similarly, let us use the symbols u_i^R and ϑ_i^R to indicate the axial displacement and the twisting rotation of the $i-$th resonant mass [11], respectively (Figure 1). We assume the following compatibility equations between the axial and twisting motions of the hosting and resonant prisms [6]

$$u_i^H = p\,\vartheta_i^H, \quad \forall i = 0, ..., N; \qquad u_i^R = p\,\vartheta_i^R, \quad \forall i = 0, ..., N-1 \tag{2.1}$$

Here, p is a coupling parameter to be determined by studying the kinematics of the P_H and P_R prisms in proximity to the reference configuration. Equation (2.1) permits to reduce the kinematics of the Maxwell chain to the axial displacements u_i^H and u_i^R of the hosting and resonant units (see [6] for more details).

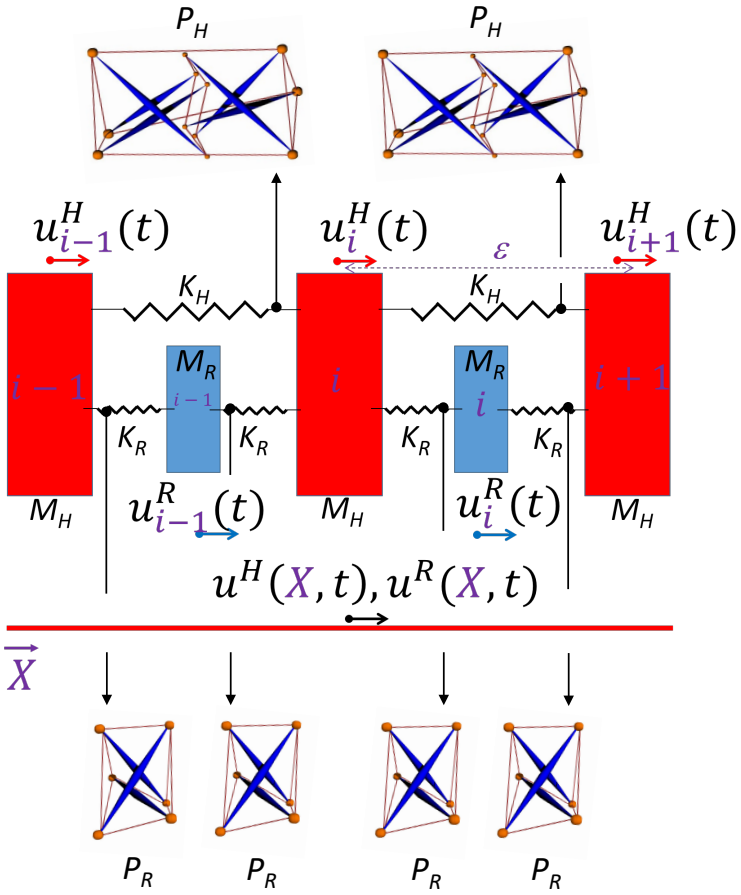

Figure 1. Graphical illustration of the tensegrity Maxwell chain.

It is an easy task to obtain the expressions of the kinetic energy $\mathcal{K}$ and the internal elastic energy

$\mathcal{U}_{int}$ of the discrete Maxwell chain model as follows:

$$\mathcal{K} \;=\; \frac{1}{2}M_H^{eq}(\dot{u}_N^H)^2 + \sum_{i=0}^{N-1}\frac{1}{2}\left[M_H^{eq}(\dot{u}_i^H)^2 + M_R^{eq}(\dot{u}_i^R)^2\right] \tag{2.2}$$

$$\mathcal{U}_{int} = \sum_{i=0}^{N-1}\frac{1}{2}\left[K_R\left(\left(u_i^H - u_i^R\right)^2 + \left(u_{i+1}^H - u_i^R\right)^2\right) \;+\; K_H\left(u_{i+1}^H - u_i^H\right)^2\right], \tag{2.3}$$

where we have employed the dot notation for time derivatives, and we have introduced the equivalent masses

$$M_H^{eq} \;=\; M_H\left(1 + \tfrac{n_H\, r_H^2}{p^2}\right), \quad M_R^{eq} \;=\; M_R\left(1 + \tfrac{n_R\, r_R^2}{p^2}\right) \tag{2.4}$$

The external energy of the Maxwell chain is given by

$$\mathcal{U}_{ext} \;=\; \mathcal{F}_{H,0}^{ext,eq}u_0^H + \sum_{i=0}^{N-1}\left[\mathcal{F}_{H,i}^{ext,eq}u_i^H(1-\delta_{0i}) + \mathcal{F}_{R,i}^{ext,eq}u_i^R\right] + \mathcal{F}_{H,N}^{ext,eq}u_N^H, \tag{2.5}$$

where the following equivalent axial forces have been introduced:

$$\mathcal{F}_{H,i}^{ext,eq} \;=\; F_{H,i}^{ext} + \frac{\mathcal{M}_{H,i}^{ext}}{p}, \quad \mathcal{F}_{R,i}^{ext,eq} \;=\; F_{R,i}^{ext} + \frac{\mathcal{M}_{R,i}^{ext}}{p} \tag{2.6}$$

$F_{H,i}^{ext}$ and $F_{R,i}^{ext}$ denote the external forces and the external twisting moments $\mathcal{M}_{H,i}^{ext}$ and $\mathcal{M}_{R,i}^{ext}$ applied to the chain.

It is worth to note that we decompose the external energy (2.5) into three addends. The first and third addends are the contributions from the external world, respectively, to the extreme left and to the extreme right-hand sides of the chain. The second addend contains the rest of the external energies. As a matter of fact, this last second addend is decomposed into two parts. The first is the contribution of the external energies due to the external forces applied to the hosting masses with $i = 1, ..., N-1$. The second is the contribution of the external energies due to the external forces applied to the resonance masses with $i = 0, ..., N-1$.

3. A continuum model for the Maxwell chain

We now introduce a one-dimensional continuum domain of length L, characterized by two displacement fields $u_H(X,t)$ and $u_R(X,t)$ (see Figure 1) as kinematic descriptors, where $X \in [0,L]$ is a spatial variable (cf. Figure 1) and $t \in [t_1,t_2]$ is the time variable. This domain represents the support of a continuum model for the Maxwell chain, which consists of a mixture of two solids: the first solid describes the hosting masses M_H of the discrete model, while the second one describes the resonance masses M_R. Both solids are defined not only for every instant of time $t \in [t_1,t_2]$ but also for every point $X \in [0,L]$ of the reference configuration. In addition, each of the two solids has its own dynamics, one being defined by the displacement field $u_H(X,t)$ and the other by the displacement field $u_R(X,t)$.

The following Piola's ansatz

$$f(X_i) = f_i, \qquad \forall i = 0, ..., N, \quad \varepsilon \ll L \quad \Rightarrow \quad \sum_{i=0}^{N} f_i \varepsilon = \int_0^L f(X) dX, \tag{3.1}$$

are assumed to link the continuum kinematic descriptors to the discrete ones introduced in the previous section, where f is either u_H or u_R, and f_i is either u_i^H or u_i^R. Such ansatzes let us identify the realizations of the continuum descriptors $u_H(X,t)$ and $u_R(X,t)$ at the points of application of the ith discrete masses M_H and M_R with the discrete descriptors $u_i^H(t)$ and $u_i^R(t)$. Making use of Eq (3.1), we are led to rewrite the kinetic energy (2.2) of the discrete Maxwell chain as follows:

$$\mathcal{K} = \sum_{i=0}^{N} \varepsilon \frac{1}{2} \left[\frac{M_H^{eq}}{\varepsilon} (\dot{u}_i^H)^2 + \frac{M_R^{eq}}{\varepsilon} (\dot{u}_i^R)^2 \right] = \int_0^L \frac{1}{2} \left[\varrho_H \dot{u}_H^2 + \varrho_R \dot{u}_R^2 \right] dX, \tag{3.2}$$

where the linear mass densities ϱ_H and ϱ_R are given by

$$\varrho_H = \frac{M_H^{eq}}{\varepsilon}, \qquad \varrho_R = \frac{M_R^{eq}}{\varepsilon}. \tag{3.3}$$

Let us now look at the continuum model as the limit for $\varepsilon \to 0$ of a sequence of discrete chain models. In correspondence to such a limit, one easily realizes that Eq (3.3) do not degenerate only if the values M_H and M_R (see also Eq (2.4)) rescale with the size ε of the unit cell of the discrete chain. We therefore assume that the values of the masses M_H and M_R tend to zero for $\varepsilon \to 0$, in such a way that the linear mass densities ϱ_H and ϱ_R remain finite.

Before we move on to identify the internal energy from Eq (2.3) of the continuum model, we need to write the displacement u_{i+1}^H of the cell $i+1$ in terms of that u_i^H of the cell i, with the use of both Piola's ansatz (3.1), adapted for the field $u^H(X,t)$, and the following Taylor's series expansion

$$u_{i+1}^H(t) = u^H(X_{i+1}, t) = u^H(X_i + \varepsilon, t) \cong u^H(X_i, t) + \varepsilon u^{H\prime}(X_i, t) + \frac{1}{2}\varepsilon^2 u^{H\prime\prime}(X_i, t) \tag{3.4}$$

Here, we have employed the prime notation for the derivatives with respect to the spatial variable X. Eq (3.4) allows us to write from Eq (2.3) the internal energy of the continuum model into the following form:

$$\begin{aligned} \mathcal{U}_{int} \quad = \quad & \sum_{i=1}^{N} \frac{\varepsilon}{2} \{ \left[\frac{K_R}{\varepsilon} \left(u^H(X_i, t) - u^R(X_i, t) \right)^2 \right] && (3.5) \\ & + \left[\frac{K_R}{\varepsilon} \left(u^H(X_i, t) + \varepsilon u^{H\prime}(X_i, t) - u^R(X_i, t) \right)^2 \right] && (3.6) \\ & + \left[\frac{K_H}{\varepsilon} \left(\varepsilon u^{H\prime}(X_i, t) \right)^2 \right] \}. && (3.7) \end{aligned}$$

which, making use of Eq (3.1), leads us finally to

$$\mathcal{U}_{int} = \int_0^L \left[\frac{1}{2} \kappa_R \left(u^H - u^R \right)^2 + \frac{1}{2} \kappa_H \left(u^{H\prime} \right)^2 \right] dX \tag{3.8}$$

The continuum stiffness constants κ_H and κ_R, which appear in Eq (3.8), are related to the discrete counterparts K_H and K_R through

$$\kappa_H = K_H\,\varepsilon, \qquad \kappa_R = 2\frac{K_R}{\varepsilon}. \tag{3.9}$$

We now go back to the identification of the continuum model as the limit for $\varepsilon \to 0$ of a sequence of discrete models. In such a limit, Eq (3.9) do not degenerate only if the values κ_H and κ_R rescale with ε according to (3.9). This implies that it must result in $K_H \to \infty$ for $\varepsilon \to 0$, in such a way that κ_H remains finite. Similarly, it must result in $K_R \to 0$ for $\varepsilon \to 0$, so that κ_R remains finite. It is worth noting that inclusion of the last term in (3.5) would include higher-order gradient terms in the final PDEs that are here neglected. Besides, quadratic terms in (2.3) have implied linear PDEs. However, for large deformation, nonlinear PDEs would be obtained by considering exponents in (2.3) higher than 2. In this general case, the difference between the formulations in the reference or in the present configurations should be considered via the so-called Piola's transformation [15]

We finally identify the external energy (2.5), making use of Piola's ansatz (3.1), for both the fields $u^H(X,t)$ and $u^R(X,t)$. We obtain the following expression of $\mathcal{U}_{ext}$ for the continuum model:

$$\begin{aligned} \mathcal{U}_{ext} &= \mathcal{F}^{ext,eq}_{H,0}(t)u^H(0,t) + \mathcal{F}^{ext,eq}_{H,N}(t)u^H(L,t), \\ &+ \sum_{i=0}^{N-1} \varepsilon \left[\frac{\mathcal{F}^{ext,eq}_{H,i}(t)}{\varepsilon} u^H(X_i,t)(1-\delta_{0i}) + \frac{\mathcal{F}^{ext,eq}_{R,i}(t)}{\varepsilon} u^R(X_i,t) \right] \end{aligned} \tag{3.10}$$

from which, making use of Eq (3.1), we get to

$$\begin{aligned} \mathcal{U}_{ext} &= \mathcal{F}^{ext,eq}_{H,0}(t)u^H(0,t) + \mathcal{F}^{ext,eq}_{H,N}(t)u^H(L,t) \\ &+ \int_0^L \left[b^H(X,t)u^H(X,t) + b^R(X,t)u^R(X,t) \right] dX. \end{aligned} \tag{3.11}$$

The distributed external forces $b^H(X,t)$ and $b^R(X,t)$, which appear in Eq (3.11), are related to the discrete counterparts $\mathcal{F}^{ext,eq}_{H,i}(t)$ and $\mathcal{F}^{ext,eq}_{R,i}(t)$ through

$$b^H(X_i,t) = \frac{\mathcal{F}^{ext,eq}_{H,i}(t)}{\varepsilon} \quad \forall i = 1,...,N-1, \qquad b^R(X_i,t) = \frac{\mathcal{F}^{ext,eq}_{R,i}(t)}{\varepsilon}, \quad \forall i = 0,...,N-1. \tag{3.12}$$

Considering again the limit for $\varepsilon \to 0$ of a sequence of discrete models, we realize that Eq (3.12) do not degenerate in correspondence to such a limit case only if the values b^H and b^R rescale with ε according to (3.12). This implies that it must result in both $\mathcal{F}^{ext,eq}_{H,i} \to 0$ and $\mathcal{F}^{ext,eq}_{R,i} \to 0$ for $\varepsilon \to 0$, in such a way that b^H and b^R remain finite for $\varepsilon \to 0$.

The action functional of the continuum model can be formulated into the following standard form (see, e.g., [17])

$$\mathcal{A} = \int_{t_1}^{t_2} \left[\mathcal{K} - \mathcal{U}_{int} + \mathcal{U}_{ext} \right], \tag{3.13}$$

where t_1 and t_2 are two times at which we prescribe that the displacement fields u^H and u^R are equal to known values u^α_H and u^α_R ($\alpha = 1, 2$), through

$$u_H(X,t_1) = u^1_H, \quad u_H(X,t_2) = u^2_H, \quad u_R(X,t_1) = u^1_R, \quad u_R(X,t_2) = u^2_R. \tag{3.14}$$

We now introduce the following action principle [17],

$$\delta\mathcal{A} = 0, \qquad \forall \delta u_H \in C_H, \qquad \forall \delta u_R \in C_R, \tag{3.15}$$

for any admissible variations C_H of u_H and C_R of u_R. It is an easy task to obtain from Eqs (3.2), (3.8), (3.11), and (3.13) the following result:

$$\begin{aligned}
\delta\mathcal{A} &= \int_{t_1}^{t_2}\left[\int_0^L \left[\delta u_H\left(-\kappa_R(u_H-u_R)+\kappa_H u_H''-\varrho_H\ddot{u}_H+b^H\right)\right]dX\right]dt \\
&+ \int_{t_1}^{t_2}\left[\int_0^L \left[\delta u_R\left(\kappa_R(u_H-u_R)-\varrho_R\ddot{u}_R+b^R\right)\right]dX\right]dt \\
&+ \int_{t_1}^{t_2}\left[\delta u_H(0,t)\left(\mathcal{F}_{H,0}^{ext,eq}(t)+\kappa_H u_H'(0,t)\right)\right]dt \\
&+ \int_{t_1}^{t_2}\left[\delta u_H(L,t)\left(\mathcal{F}_{H,L}^{ext,eq}(t)-\kappa_H u_H'(L,t)\right)\right]dt.
\end{aligned} \tag{3.16}$$

Invoking the arbitrariness of the variations in (3.15), we can finally derive the following PDEs ruling the dynamic problem of the continuum model:

$$\kappa_R(u_H-u_R)-\kappa_H u_H''+\varrho_H\ddot{u}_H-b^H=0 \tag{3.17}$$

$$-\kappa_R(u_H-u_R)+\varrho_R\ddot{u}_R-b^R=0 \tag{3.18}$$

which are accompanied by the BCs

$$u_H(0,t)=u_{H0}(t) \qquad or \qquad \kappa_H u_H'(0,t)=-\mathcal{F}_{H,0}^{ext,eq}(t) \tag{3.19}$$

$$u_H(L,t)=u_{HL}(t) \qquad or \qquad \kappa_H u_H'(L,t)=\mathcal{F}_{H,L}^{ext,eq}(t). \tag{3.20}$$

Let us now introduce plane wave solutions for the displacement fields $u_H(X,t)$ and $u_R(X,t)$, through

$$u_H=\mathrm{Re}\left\{u_0^H\exp\left[I\left(\omega t-k_w X\right)\right]\right\}, \quad u_R=\mathrm{Re}\left\{u_0^R\exp\left[I\left(\omega t-k_w X\right)\right]\right\} \tag{3.21}$$

where Re indicates the real part operator; I is the imaginary unit; u_0^H, u_0^R, ω, and k_w, respectively, denote the complex amplitudes, the angular frequency, and the wave number of the traveling waves. Making use of Eq (3.21), we easily obtain (neglecting all the external forces and the external energy terms) the following dispersion relation of the continuum model

$$\omega_{Moc,Mac}\left(k_w\right)=\sqrt{\frac{f_M(k_w)\pm\Delta_M\left(k_w\right)}{2\varrho_H\varrho_R}} \tag{3.22}$$

where the function $f_M(k_w)$ and the discriminant $\Delta_M\left(k_w\right)$ have the expressions given below

$$f_M(k_w) = (\varrho_H+\varrho_R)\kappa_R+\varrho_R\kappa_H k_w^2 \tag{3.23}$$

$$\Delta_M\left(k_w\right) = \sqrt{\left[f_M(k_w)\right]^2-4\varrho_H\varrho_R\kappa_R\kappa_H k_w^2}. \tag{3.24}$$

In the limit $\varepsilon \to 0$, Eq (3.22) reduce to the form

$$\omega_{Mac} \cong k_w \sqrt{\frac{\kappa_H}{\varrho_H + \varrho_R}}, \tag{3.25}$$

$$\omega_{Moc} \cong \sqrt{\frac{\kappa_R(\varrho_H + \varrho_R)}{\varrho_H \varrho_R}}. \tag{3.26}$$

Making use of the positions (3.3) and (3.9), it is easily verified that both the Eqs (3.25) and (3.26) reduce to Eq (25), in the reference [6], of the discrete model, which has been presented to provide the value of the circular frequency of the optic branch for $k_w = 0$.

It is useful to apply the above formulas to the micro-scale physical models of the Maxwell chain studied in [6]. Such models employ P_R prisms with a 5.5 mm height in the reference configuration, equilateral triangular bases with an 8.7 mm edge, 0.28 mm Spectra strings (5.48 GPa Young modulus), and 0.8 mm Ti6Al4V bars (120 GPa Young modulus). In addition, they use P_H prisms showing 11 mm height in the reference configuration, equilateral triangular bases with a 6.11 mm edge, Spectra strings and Ti6Al4V bars identical to those of the P_R prisms (we refer the reader to [6] for more detailed information about such units). The masses forming the above models are circular discs, such that $M_H = 16.03$ grams and $M_R = 4$ grams ($n_H = n_R = 1/2$). The study presented in [6] estimates $K_H = 61.04$ N/mm, $K_R = 13.70$ N/mm, and $p \approx 2.33$ mm/rad.

Graphical illustrations of the dispersion relations exhibited by discrete and continuum models of the chain under examination are provided in Figure 2, by distinguishing two different cases: discrete and continuum systems in which the longitudinal and twisting motions of the P_H and P_R prisms are coupled, according to Eq (2.1), as well as discrete and continuum systems in which the same prisms are free to tangentially slide against the lumped masses, so as that the twisting rotations of the tensegrity units are not transferred to the masses (uncoupled system). In the first case, we have $M_H^{eq} = 349.51$ grams and $M_R^{eq} = 24.85$ grams, while in the second case, it results in $M_H^{eq} = M_H$ and $M_R^{eq} = M_R$. Figure 2 shows that the acoustic and optic branches forming the dispersion relations of the continuum systems correctly reduce to the analogous branches of the discrete systems in the long wavelength regime ($k_w \to 0$). In the coupled system we predict $\omega_{Moc}(0) = 173$ Hz, while in the uncoupled system, we predict $\omega_{Moc}(0) = 465$ Hz.

4. Analytic solutions of the wave equation

Let us derive the wave equation of the continuum model of the Maxwell chain, by making use of the results derived in the previous section. We start by rewriting Eq (3.21) into the following form:

$$u_H = \mathrm{Re}\left\{\bar{u}_0^H(X)\exp\left[I\left(\omega t\right)\right]\right\} + u_S^H(X), \quad u_R = \mathrm{Re}\left\{\bar{u}_0^R(X)\exp\left[I\left(\omega t\right)\right]\right\} + u_S^R(X), \tag{4.1}$$

where now $\bar{u}_0^H(X)$ and $\bar{u}_0^R(X)$ are unknown functions of the spatial coordinate X, and $u_S^H(X)$ and $u_S^R(X)$ are those displacement functions produced by a static load at the boundary and assuming zero external distributed forces ($b_H = b_R = 0$). Thus, Eqs (3.17) and (3.18) yield,

$$\kappa_R(u_S^H - u_S^R) - \kappa_H u_S^{H\prime\prime} = 0 \tag{4.2}$$

$$-\kappa_R(u_S^H - u_S^R) = 0 \tag{4.3}$$

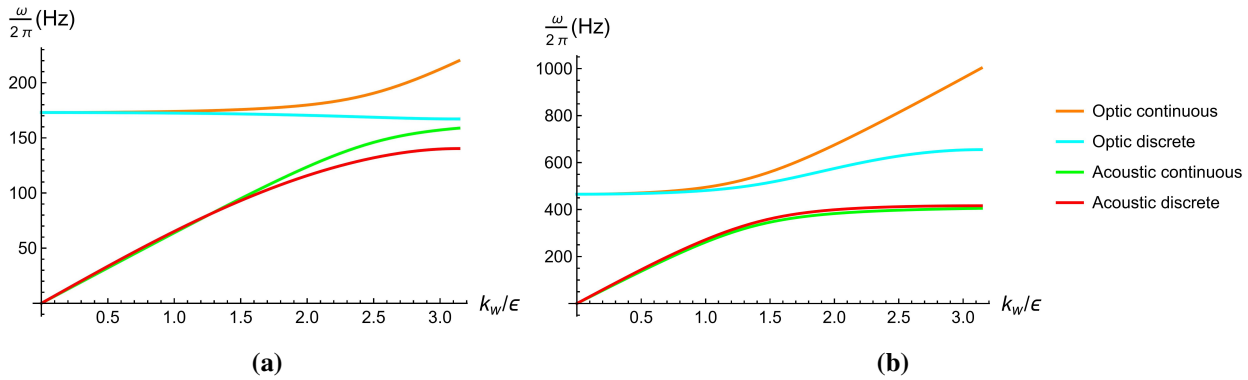

Figure 2. A comparison between the dispersion relations of the discrete and continuous models for the physical model of the Maxwell chain with coupled (a) and uncoupled (b) longitudinal and twisting motions.

and $u_S^H(X)$ and $u_S^R(X)$ are solved once a particular set of boundary conditions are considered. Keeping this in mind, one can write Eqs (3.17) and (3.18) making use of Eq (4.1), to obtain

$$\kappa_R(\bar{u}_0^H - \bar{u}_0^R) - \kappa_H \bar{u}_0^{H\prime\prime} + \varrho_H \omega^2 \bar{u}_0^H = 0 \tag{4.4}$$

$$-\kappa_R(\bar{u}_0^H - \bar{u}_0^R) + \varrho_R \omega^2 \bar{u}_0^R = 0. \tag{4.5}$$

The insertion of Eq (4.5) into Eq (4.4) leads us to the second-order linear homogeneous differential equation with respect to the spatial coordinate X

$$\kappa_H \bar{u}_0^{H\prime\prime} + \omega^2 \bar{\varrho}_H \bar{u}_0^H = 0 \tag{4.6}$$

where we have introduced the equivalent mass density

$$\bar{\varrho}_H = \frac{\kappa_R(\varrho_R + \varrho_H) - \varrho_R \varrho_H \omega^2}{\kappa_R - \varrho_R \omega^2} \tag{4.7}$$

Eq (4.6) admits the following general solution:

$$\bar{u}_0^H = \mathrm{Re}\left\{c_1 \exp\left[\alpha_1 X\right] + c_2 \exp\left[\alpha_2 X\right]\right\} \tag{4.8}$$

where we introduced the integration constants c_1 and c_2, to be determined through the competent boundary conditions, and we set

$$\alpha_{1,2} = \pm\, \omega \sqrt{-\frac{\bar{\varrho}_H}{\kappa_H}}. \tag{4.9}$$

Moving on to determine analytic solutions for $\bar{u}_0^R(X)$, we now insert Eq (4.8) into Eq (4.5), obtaining

$$\bar{u}_0^R = \frac{\kappa_R}{\varrho_R\, \omega^2 + \kappa_R} \left[\mathrm{Re}\left\{c_1 \exp\left[\alpha_1 X\right] + c_2 \exp\left[\alpha_2 X\right]\right\}\right] \tag{4.10}$$

Let us now determine the constants c_1 and c_2 in the particular case of a chain lying vertically in space, which is subject to a mass M applied to the top end ($X = L$) and a sinusoidal displacement excitation at the bottom end ($X = 0$). The base excitation has an amplitude of u_0 and can be written as

$$u_H(0, t) = u_0 \cos(\omega t) \tag{4.11}$$

It is useful to separate the dynamic and static parts of Eq (4.1). For what concerns the dynamic part, we analyze the boundary conditions

$$\bar{u}_0^H(0) = u_0 \qquad \bar{u}_0^{H\prime}(L) = 0. \tag{4.12}$$

which, once inserted into Eq (4.8), leads us to compute the integration constants c_1 and c_2, and to obtain the dynamic amplitude of the hosting displacement field

$$\bar{u}_0^H = u_0 \,\mathrm{Re}\left\{\sec\left[\alpha_1 L\right]\cos\left[\alpha_1(L-X)\right]\right\} \tag{4.13}$$

and from Eq (4.10) that of the resonant one,

$$\bar{u}_0^R = \frac{\kappa_R\, u_0}{\varrho_R\,\omega^2 + \kappa_R}\mathrm{Re}\left\{\sec\left[\alpha_1 L\right]\cos\left[\alpha_1(L-X)\right]\right\} \tag{4.14}$$

For what concerns the static terms u_S^H and u_S^R, we observe that Eq (4.3) implies the following result in static equilibrium conditions:

$$\kappa_R(u_S^H - u_S^R) = 0. \tag{4.15}$$

which is accompanied by the static boundary condition

$$u_S^H(0) = 0 \tag{4.16}$$

On the other hand, in the example under consideration, it is a simple task to obtain the following differential equation for u_S^H [20]

$$u_S^{H\prime}(L) = -\frac{Mg}{\kappa_H} \tag{4.17}$$

where g is the gravity acceleration. Making use of Eqs (4.16) and (4.17) in Eq (4.15), we finally obtain

$$u_S^H(X) = u_S^R(X) = -\frac{Mg}{\kappa_H}X \tag{4.18}$$

We are now able to cast Eq (4.1) into the following form:

$$u_H(X,t) = u_0 \,\mathrm{Re}\left\{\sec\left[\alpha_1 L\right]\cos\left[\alpha_1(L-X)\right]\exp\left[I\,(\omega t)\right]\right\} - \frac{Mg}{\kappa_H}X \tag{4.19}$$

$$u_R(X,t) = \frac{\kappa_R\, u_0}{\varrho_R\,\omega^2 + \kappa_R}\,\mathrm{Re}\left\{\sec\left[\alpha_1 L\right]\cos\left[\alpha_1(L-X)\right]\exp\left[I\,(\omega t)\right]\right\} - \frac{Mg}{\kappa_H}X \tag{4.20}$$

Since we are assuming $\kappa_H > 0$ (cf. Section 2), Eqs (4.19) and (4.20), in association with the positions (4.9), let us conclude that one obtains periodic harmonic solutions for u_H and u_R only when α_1 and α_2 are imaginary ($\bar{\varrho}_H > 0$). Oppositely, we obtain decaying solutions when α_1 and α_2 are real ($\bar{\varrho}_H < 0$). The frequency bandgap region obviously corresponds to $\bar{\varrho}_H < 0$, since in this case the system supports wave solutions that exponentially decay when X approaches L [18, 19]. It is easily verified that the values of $\omega > 0$ such that $\bar{\varrho}_H < 0$ are contained in the interval comprised between zero and the frequency ω_{Moc} provided by Eq (3.26). Such a result provides validation of the dispersion relation derived in the previous section, and highlights that the analyzed chain can be effectively employed as an isolation device for vertical vibrations of the top mass M. It is not difficult to generalize the results obtained in the present section to the case in which the examined system is under the action of a not-negligible self-weight. For such an example, indeed, the dynamic parts of u_H and u_R remains unchanged as compared to the present case, while the static parts of these functions will assume a quadratic expression with respect to X [20].

5. Conclusions

We have derived a continuum model for a Maxwell-type mass–spring chain with tensegrity architecture [12, 13], which exhibits $\theta = 1$ tensegrity prisms [14] arranged in parallel with T3 prisms [16] and lumped masses. When compared to the discrete model presented in [19], the theory formulated in the present work is useful to obtain analytic solutions for the wave propagation problem of the analyzed system in the high wave-length regime, where structural applications are relevant [21, 22]. Such a feature has been demonstrated through the analysis of a physical example, which refers to the vibration isolation problem of a mass, e.g., a device to be protected against mechanical vibrations in a hospital or another essential building. It is worth noting that the mass–spring chain studied in this work exhibits internal resonance properties that can be employed to widen the frequency bandgap width of the system, as compared to the case of a diatomic tensegrity mass–spring chain, where such a width can only be tuned by playing with mass and stiffness contrasts between the elements of the unit cell [23].

The research presented in this work paves the way for the design of novel tensegrity metamaterials serving as next-generation vibration isolation devices. Such systems will exhibit properties that can be easily adjusted to the structure to be protected due to the tunability of the frequency bandgap region [19]. The presence of geometrical and mechanical nonlinearities in such devices will be studied through future research, accounting, e.g., for the presence of superelastic cables made of shape memory alloys [24] and higher order terms in the internal an kinetic energies [25, 26]. Their use in forming anisotropic and/or porous metamaterials [27, 28], energy harvesters [29], and sensors and actuators for structural health monitoring [30] will also be investigated in future studies.

Author contributions

L.P. formulated the initial idea for the continuum model, while F.F., J.d.C.M., and R.Z.C. conceived the tensegrity modeling. L.P. and F.F. led the conceptualization, idealization, and supervision phases of the project. F.F. provided funding. J.d.C.M. led the development of the analytical results, while R.Z.C. led the numerical analysis of the physical models. All authors contributed to the first draft and the revised version of the manuscript.

Use of AI tools declaration

The authors declare they have not used Artificial Intelligence (AI) tools in the creation of this article.

Acknowledgements

This research has been funded under the National Recovery and Resilience Plan (NRRP), by the European Union–NextGenerationEU, within the project with grant number P2022CR8AJ (FF PI). This research has also been funded by the NextGenerationEU PRIN2022 research projects with grant numbers 20224LBXMZ (FF PI) and 2022P5R22A (“Ricerca finanziata dall’Unione Europea–Next Generation EU”). FF and JdCM also acknowledge the support by the Italian Ministry of Foreign Affairs and International Cooperation within the Italy-USA Science and Technology Cooperation

Program 2023–2025, Project “Next-generation green structures for natural disaster-proof buildings” (grant No. US23GR15).

Conflict of interest

The authors declare that there is no conflict of interest.

References

1. M. Kadic, G. W. Milton, M. van Hecke, M. Wegener, 3D metamaterials, *Nat. Rev. Phys.*, **1** (2019), 198–210. https://doi.org/10.1038/s42254-018-0018-y
2. Y. Pennec, J. O. Vasseur, B. Djafari-Rouhani, L. Dobrzyński, P. A. Deymier, Two-dimensional phononic crystals: Examples and applications, *Surf. Sci. Rep.*, **65** (2010), 229–291. https://doi.org/10.1016/j.surfrep.2010.08.002
3. M. Mazzotti, I. Bartoli, M. Miniaci, Modeling Bloch waves in prestressed phononic crystal plates, *Front Mater*, **6** (2019), 74. https://doi.org/10.3389/fmats.2019.00074
4. A. Bergamini, M. Miniaci, T. Delpero, D. Tallarico, B. Van Damme, G. Hannema, et al., Tacticity in chiral phononic crystals, *Nat Commun*, **10** (2019), 4525. https://doi.org/10.1038/s41467-019-12587-7
5. A. S. Gliozzi, M. Miniaci, A. Chiappone, A. Bergamini, B. Morin, E. Descrovi, Tunable photo-responsive elastic metamaterials, *Nat Commun*, **11** (2020), 2576. https://doi.org/10.1038/s41467-020-16272-y
6. L. Placidi, J. de Castro Motta, F. Fraternali, Bandgap structure of tensegrity mass-spring chains equipped with internal resonators, *Mech. Res. Commun.*, **137** (2024), 104273. https://doi.org/10.1016/j.mechrescom.2024.104273
7. E. Barchiesi, S. Khakalo, Variational asymptotic homogenization of beam-like square lattice structures, *Math Mech Solids*, **24** (2019), 3295–3318. https://doi.org/10.1177/1081286519843155
8. E. Turco, A. Misra, M. Pawlikowski, F. dell’Isola, F. Hild, Enhanced Piola–Hencky discrete models for pantographic sheets with pivots without deformation energy: numerics and experiments, *Int. J. Solids. Struct.*, **147** (2018), 94–109. https://doi.org/10.1016/j.ijsolstr.2018.05.015
9. E. Barchiesi, S. R. Eugster, L. Placidi, F. dell’Isola, Pantographic beam: a complete second gradient 1D-continuum in plane, *Z. Angew. Math. Phys.*, **70** (2019), 1–24. https://doi.org/10.1007/s00033-018-1046-2
10. E. Turco, E. Barchiesi, I. Giorgio, F. dell’Isola, A Lagrangian Hencky-type non-linear model suitable for metamaterials design of shearable and extensible slender deformable bodies alternative to Timoshenko theory, *Int. J. Non. Linear. Mech.*, **123** (2020), 103481. https://doi.org/10.1016/j.ijnonlinmec.2020.103481
11. F. dell’Isola, L. Rosa, C. Wozniak, Dynamics of solids with microperiodic nonconnected fluid inclusions, *Arch. Appl. Mech.*, (1997), 215–228.

12. F. Fabbrocino, G. Carpentieri, A. Amendola, R. Penna, F. Fraternali, Accurate numerical methods for studying the nonlinear wave-dynamics of tensegrity metamaterials, *Eccomas Procedia Compdyn*, (2017), 3911–3922. https://doi.org/10.7712/120117.5693.17765
13. F. Fabbrocino, G. Carpentieri, Three-dimensional modeling of the wave dynamics of tensegrity lattices, *Compos. Struct.*, **173** (2017), 9–16. https://doi.org/10.1016/j.compstruct.2017.03.102
14. I. Mascolo, A. Amendola, G. Zuccaro, L. Feo, F. Fraternali, On the geometrically nonlinear elastic response of class $\theta = 1$ tensegrity prisms, *Front Mater*, **5** (2018), 16. https://doi.org/10.3389/fmats.2018.00016
15. F. dell'Isola, S. R. Eugster, R. Fedele, P. Seppecher, Second-gradient continua: From Lagrangian to Eulerian and back, *Math. Mech. Solids.*, **27** (2022), 2715–2750. https://doi.org/10.1177/10812865221078822
16. R. E. Skelton, M. C. de Oliveira, *Tensegrity Systems*, New York: Springer, 2010.
17. L. D. Landau, E. M. Lifshitz, *Mechanics, Third Edition: Volume 1 (Course of Theoretical Physics)*, Oxford: Butterworth-Heinemann, 1976.
18. S. J. Mitchell, A. Pandolfi, M. Ortiz, Investigation of elastic wave transmission in a metaconcrete slab, *Mech. Mater.*, **91** (2015), 295–303. https://doi.org/10.1016/j.mechmat.2015.08.004
19. L. Placidi, F. Di Girolamo, R. Fedele, Variational study of a Maxwell–Rayleigh-type finite length model for the preliminary design of a tensegrity chain with a tunable band gap, *Mech. Res. Commun.*, **136** (2024), 104255. https://doi.org/10.1016/j.mechrescom.2024.104255
20. F. Beer, E. Johnston, J. DeWolf, *Mechanics of Materials*, 5th Eds, New York: McGraw-Hill, 1999.
21. R. Luciano, H. Darban, C. Bartolomeo, F. Fabbrocino, D. Scorza, Free flexural vibrations of nanobeams with non-classical boundary conditions using stress-driven nonlocal model, *Mech. Res. Commun.*, **107** (2020), 103536. https://doi.org/10.1016/j.mechrescom.2020.103536
22. H. Darban, R. Luciano, A. Caporale, F. Fabbrocino, Higher modes of buckling in shear deformable nanobeams, *Int. J. Eng. Sci.*, **154** (2020), 103338. https://doi.org/10.1016/j.ijengsci.2020.103338
23. A. Amendola, A. Krushynska, C. Daraio, N. M. Pugno, F. Fraternali, Tuning frequency band gaps of tensegrity metamaterials with local and global prestress, *Int. J. Solids. Struct.*, **155** (2018), 47–56. https://doi.org/10.1016/j.ijsolstr.2018.07.002
24. F. Fraternali, J. de Castro Motta, Mechanics of superelastic tensegrity braces for timber frames equipped with buckling-restrained devices, *Int. J. Solids. Struct.*, **281** (2023), 112414. https://doi.org/10.1016/j.ijsolstr.2023.112414
25. F. Cornacchia, F. Fabbrocino, N. Fantuzzi, R. Luciano, R. Penna, Analytical solution of cross-and angle-ply nano plates with strain gradient theory for linear vibrations and buckling, *Mech. Adv. Mater. Struct.*, **28** (2021), 1201–1215. https://doi.org/10.1093/isle/isab051
26. G. Mancusi, F. Fabbrocino, L. Feo, F. Fraternali, Size effect and dynamic properties of 2D lattice materials, *Compos. B. Eng.*, **112** (2017), 235–242. https://doi.org/10.1016/j.compositesb.2016.12.026
27. A. Amendola, J. de Castro Motta, G. Saccomandi, L. Vergori, A constitutive model for transversely isotropic dispersive materials, *P Roy Soc A-math Phy*, **480** (2024), 20230374. https://doi.org/10.1098/rspa.2023.0374

28. J. de Castro Motta, V. Zampoli, S. Chiriţă, M. Ciarletta, On the structural stability for a model of mixture of porous solids, *Math. Methods Appl. Sci.*, **47** (2024), 4513–4529. https://doi.org/10.1002/mma.9825

29. K. Li, P. Rizzo, Energy harvesting using arrays of granular chains and solid rods, *J. Appl. Phys.*, **117** (2015), 215101. https://doi.org/10.1063/1.4921856

30. R. Misra, H. Jalali, S. J. Dickerson, P. Rizzo, Wireless module for nondestructive testing/structural health monitoring applications based on solitary waves, *Sensors*, **20** (2020), 3016. https://doi.org/10.3390/s20113016

AIMS Press